Two-Phase Flow Maldistribution and Mitigation in Polymer Electrolyte Fuel Cells

Suman Basu

Chao-Yang Wang

Electrochemical Engine Center,
The Pennsylvania State University,
University Park, PA 16802;
Department of Mechanical Engineering,
The Pennsylvania State University,
University Park, PA 16802

Ken S. Chen
Engineering Sciences Center,
Sandia National Laboratories,
Albuquerque, NM 87185-0836

Flow maldistribution among polymer electrolyte fuel-cell (PEFC) channels is of concern because this leads to nonuniform distributions of fuel and oxidizer, which in turn result in nonuniform reaction rates in the catalyst layers and thus detrimentally affect PEFC performance and durability. Channels with low flow rates risk flooding by liquid water. This can cause catalyst support corrosion and hence the undesirably accelerated aging of PEFCs. Multiphase flow computations are performed to examine the effects of gas diffusion layer (GDL) intrusion and manifold design on reducing flow maldistribution. Velocity field, hydrodynamic pressure, and liquid saturations are computed in the parallel gas channels using the multiphase-mixture formulation in order to quantify the flow nonuniformity or maldistribution among PEFC channels. It is shown that, when channel flow is in single phase, employing two splitter plates in the header manifold can bring down the flow maldistribution to less than half of that for the case with 20% area maldistribution due to the GDL intrusion. When channel flow occurs in the two-phase regime, the liquid-water front can be pushed downstream and the effect of GDL intrusion on the maximum liquid saturation can be decreased by more than one-third by using flow splitters.
[DOI: 10.1115/1.2971124]

Introduction

In a polymer electrolyte fuel cell (PEFC), it is important to ensure an even distribution of reactants in all flow channels. The deformable gas diffusion layer (GDL) material is compressed during PEFC assembly to minimize the contact resistance between GDL and bipolar plate. Clamping is also necessary to make the PEFC leak proof. This compression is higher near the edges of the cell, making GDL material intrude more into the PEFC gas channels there. This GDL intrusion at the side channels causes an area maldistribution among the channels, exacerbating the inherent flow maldistribution problem in multiple parallel channels fed from a single header. Maldistribution of flow in the parallel channels leads to direct and indirect losses. Less flow means less reactant to the reaction sites in the catalyst layers and reduced ability to transport the product water away. Much of the product water crosses over to the anode side due to back diffusion across the thin membranes, causing anode flooding and fuel starvation. In the absence of hydrogen fuel, the carbon support in the cathode catalyst layer is subject to corroding rapidly. The indirect problem is that less flow would mean less momentum and hence more susceptibility to blockage by liquid water due to water vapor condensation. This leads to a serious loss of PEFC efficiency as the whole channel may be lost due to blockage. If a channel is permanently blocked, it is obvious that no reactant will reach the reaction sites. Even if a channel is not permanently blocked, fluctuation in the output power results, caused by the cycle of liquid clogging and subsequent flush-out in the flooded channel. Hence, for a PEFC to maintain stable performance, channel flooding (which refers to excessive presence of liquid water in the channels) must be avoided.

Achieving a uniform distribution is a challenging task in parallel channels, even with a single-phase flow at the inlet. From their experimental investigation of single-phase flow in parallel microchannels, Yin et al. [1] developed a pressure-drop model for the whole heat exchanger. Remarkably, the Moody chart was found to be valid inside the channels. Maharudrayya et al. [2] presented a one-dimensional analytical solution of pressure-drop for *U*- and *Z*-type parallel channels in single-phase flow. This model can be used to select dimensions for the headers and channels in order to minimize the maldistribution of the gas flow at the inlet. For an ideal fluid, *Z*-type configuration should give a uniform distribution of flow in all the channels, but for a real fluid flowing through imperfect parallel channels due to GDL intrusion, etc., the flow maldistribution can be severe. Hrnjak [3] addressed the problem of maldistribution of single-phase flow in parallel microchannel heat exchangers. One approach is to employ a branched inlet header, as shown in Fig. 1(*a*). In the case of PEFCs, branching may prove to be effective although this would require more volume and pressure penalty is high. Nevertheless, this approach would require a fundamental change in fuel-cell design. Another approach is to use a conical header, as sketched in Fig. 1(*b*). This configuration is also very efficient with regard to the pressure-drop. However, this requires a fundamental change in the PEFC design and the packing efficiency of the PEFC stack would de-

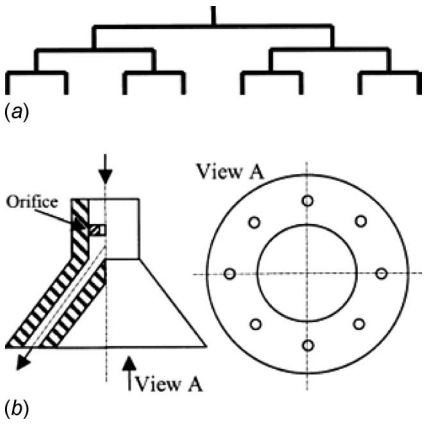

Fig. 1 (*a*) Branched header; (*b*) Conical header

Manuscript received June 13, 2007; final manuscript received October 8, 2007; published online May 12, 2009. Review conducted by Ugur Pasaogullari. Paper presented at the 5th International Fuel Cell Science Engineering and Technology Conference (FUELCELL2007), Brooklyn, NY, June 18–20, 2007.

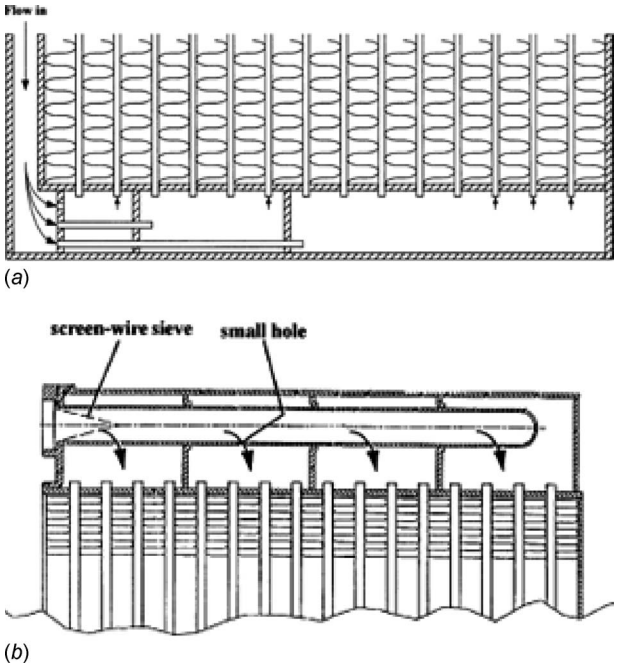

Fig. 2 (*a*) **Heat exchanger header by Toshihara [5];** (*b*) **Inlet distributor tube with sieve mesh distribution [6]**

crease substantially. Webb and Chung [4] studied the two-phase flow distribution in parallel channels for different headers and channel geometries. This investigation shows that employing obstacles at the inlet alleviates maldistribution. Yet another approach is to use branch headers to direct the flow to different sets of channels. Figure 2 presents two such branched header designs patented by Toshihara [5] and Haussman [6]. Based on these works, the use of a small diameter distribution tube with small spaced exit holes along its length seems a viable option for obtaining a good flow distribution.

Channel flooding in PEFCs has received increased attention [7–18]. Two-phase flow characteristics in the PEFC channels were investigated experimentally by Lee et al. [1] While they proposed a friction factor closely resembling that for a laminar flow in a circular channel, their investigation considered a single-point injection of liquid, which is not the case for a PEFC channel. Neither the channel flooding nor the flow instability was investigated.

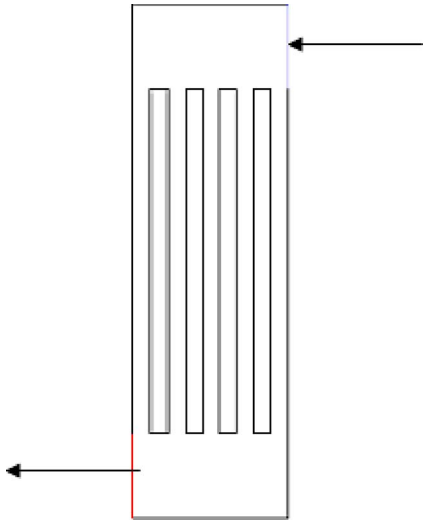

Fig. 3 Conventional geometry of channels

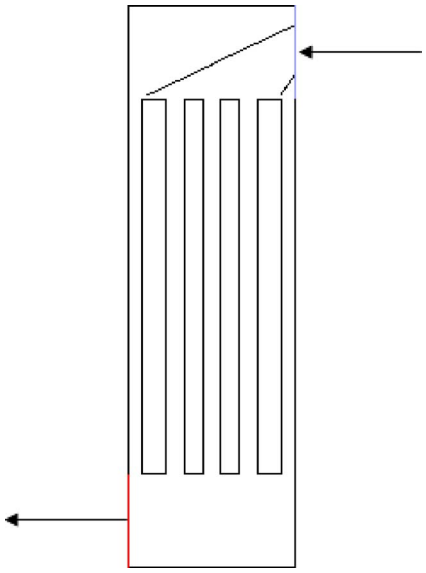

Fig. 4 Proposed geometry

Lee et al. validated their results even in the case of multiphase flow, using a gas-phase Reynolds number. Along the same line, Barreras et al. [8] recently studied flow maldistribution in parallel microchannels of PEFCs experimentally and numerically. In their study, the inlet flow enters the channels preferentially. They attributed the nonhomogeneity partly to the formation of recirculation bubbles at the inlet and concluded that making the angle of the inlet header more than the right angle to the parallel channels alleviates maldistribution. Single phase flow in the channel has been used widely in the gas channel for design purposes [9,10,18], but experiments [15,16] have shown that flow in the gas channels is not single phase. Researchers have tried to calculate the dry length of a gas channel analytically [11] as a design tool. Others used the conventional two fluid models [12–14] to simulate two-phase flow in the gas channels. Unfortunately, these models are computationally expensive and incompatible with the single fluid transport model in other components of the PEFC.

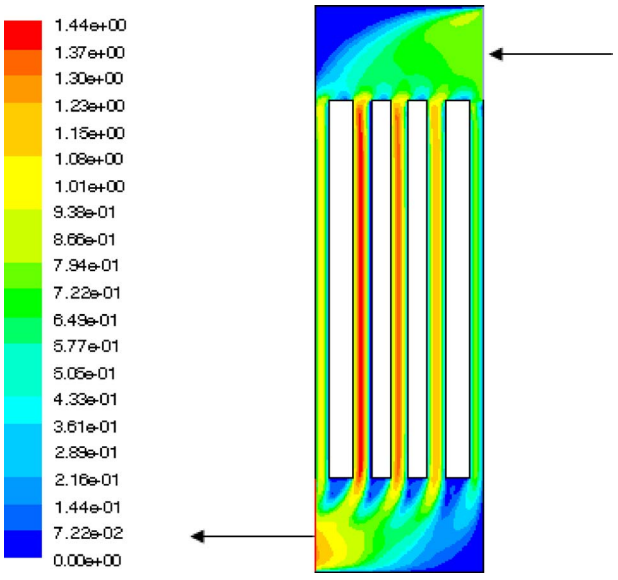

Fig. 5 Velocity (m/s) contour for channels with area maldistribution

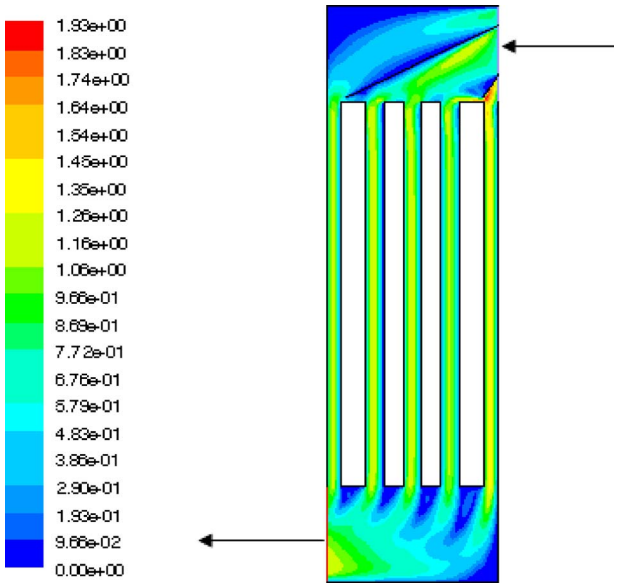

Fig. 6 Velocity (m/s) contour for channels with area maldistribution with splitters

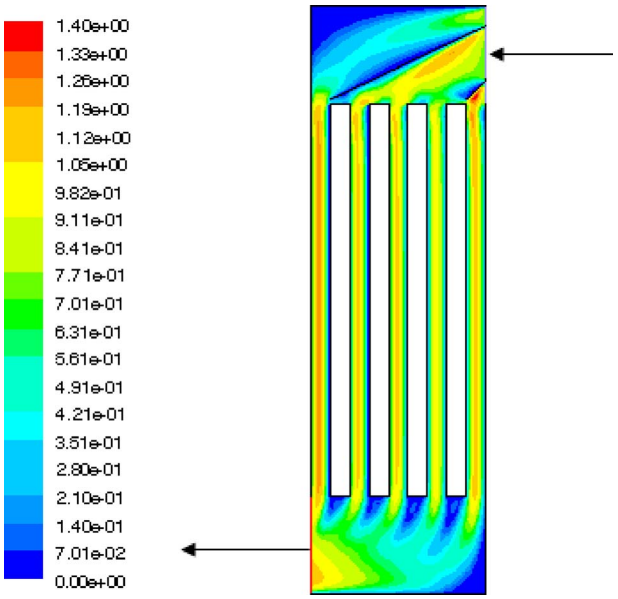

Fig. 8 Velocity (m/s) contour for perfect channels with splitters

In the present work, we perform multiphase flow computations to study the effects of GDL intrusion and manifold design on reducing flow maldistribution. Specifically, we compute the velocity field, hydrodynamic pressure, and liquid saturations along the parallel gas channels using the multiphase-mixture formulation.

Numerical Model

Model Development. Two-phase mixture flow and water transport in the channels are governed by the laws of momentum, mass, and species conservation. The multiphase-mixture model (M^2) model [19–23] is used to model the two-phase flow in the channels.

In mixture continuity equation,

$$\nabla \cdot (\rho \boldsymbol{u}) = S_m \tag{1}$$

In mixture momentum conservation,

$$\rho \boldsymbol{u} = -\frac{K}{\nu} \nabla P \tag{2}$$

In water species conservation,

$$\nabla \cdot (\gamma_c \boldsymbol{u} C^W) = \nabla \cdot (D_g^{W,\text{eff}} \nabla C_g^W) - \nabla \cdot \left[\left(\frac{m f_l^W}{M^k} - \frac{C_g^W}{\rho_g} \right) \boldsymbol{j}_l \right] + S_w \tag{3}$$

The mass source term in Eq. (1) is the net mass source in the cathode gas channels due to oxygen diffusing out of the channels and water diffusing into the channels. In reality, product water and heat are injected into the channel from the GDL-channel interface and a proportional amount of oxygen is transported through the same interface. As we model only the gas channel, the excess mass is added to the continuity equation as a source term. The source term is calculated as [21],

$$S_m = (M^w S_w - M^{O_2} S_{O_2}) \tag{4}$$

where M^w and M^{O_2} are the molecular weights of water and oxygen, respectively. The water and oxygen production rate (S_w and S_{O_2}) can be calculated from the Faraday relations as follows:

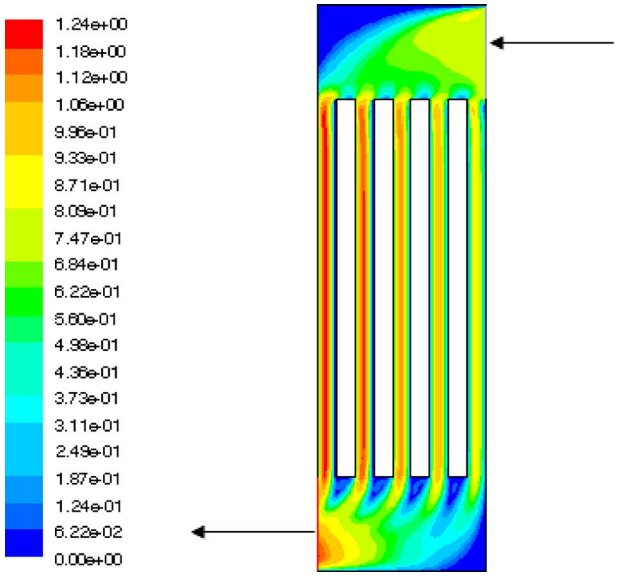

Fig. 7 Velocity (m/s) contour for perfect channels

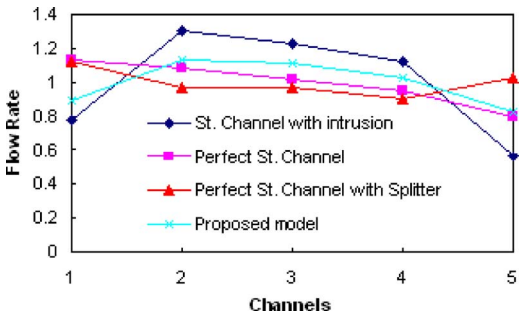

Fig. 9 Normalized flow through the channels for different configuration

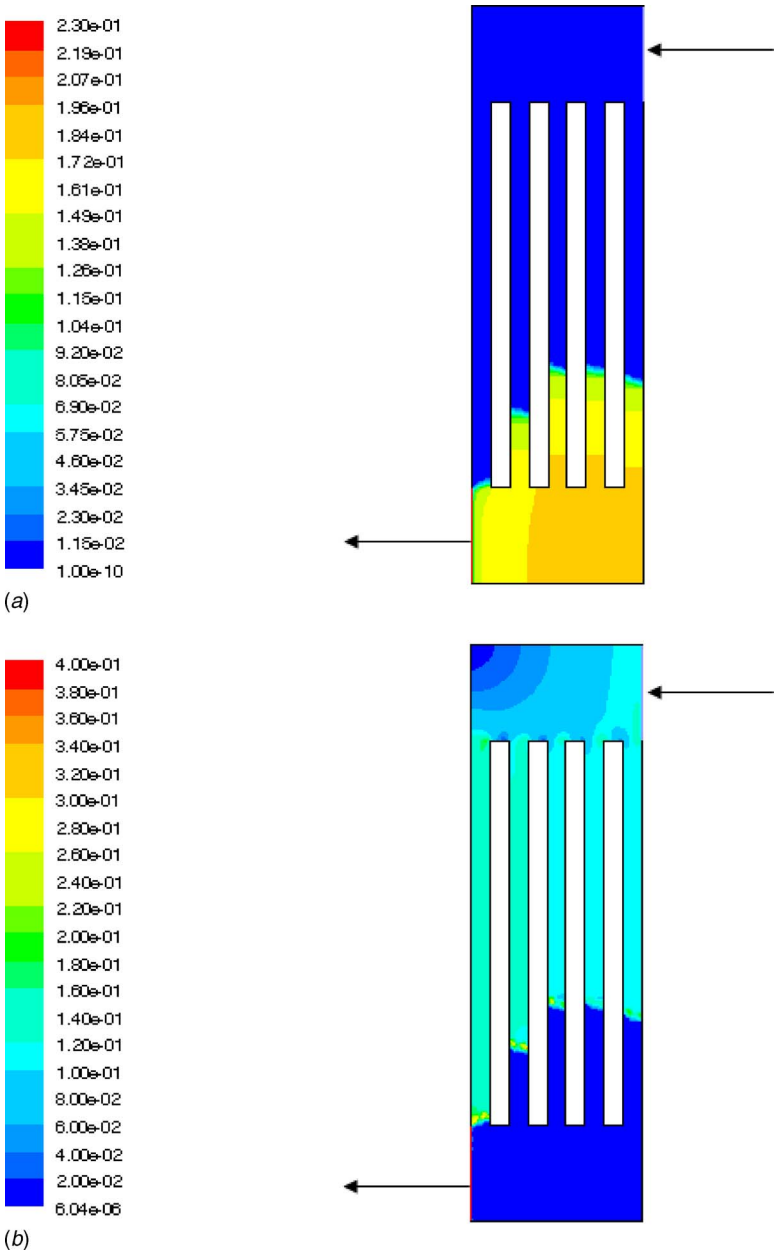

Fig. 10 (*a*) **Saturation contour (no intrusion, *I*=0.2 A/cm^2, St=4.0); (*b*) Velocity (m/s) contour (no intrusion, *I*=0.2 A/cm^2, St=4.0)**

$$S_w = \frac{(1+2\alpha)IA_{\text{mem}}}{2FV_{\text{channel}}} \quad \text{and} \quad S_{O_2} = -\frac{IA_{\text{mem}}}{4FV_{\text{channel}}} \tag{5}$$

where α is the net water transport coefficient per proton, which describes the combined effect of water diffusion and electro-osmotic drag [22] and usually has a positive value. Assuming the net water transport coefficient to be equal to zero [23], we get after some algebraic manipulation

$$S_m = \frac{M^{H_2}IA_{\text{mem}}}{2FV_{\text{channel}}} \tag{6}$$

The capillary diffusivity is calculated following Wang et al. [23]. However, simple order of magnitude analysis shows that the Peclet number based on molecular diffusion in the channel is $\approx 10^4$, while the capillary diffusion is three to four orders of magnitude less than the molecular diffusion. Therefore, the contributions from the last two terms in the right hand side of Eq. (3) are negligible.

In Eqs. (1) and (2), the mixture density is defined using the M^2 formulation [19,20]:

$$\rho = \rho_l s + \rho_g(1-s) \tag{7}$$

where ρ_l is the density of liquid water, ρ_g is the density of vapor, and s is liquid saturation defined by

$$s = \frac{C^W - C^W_{\text{sat}}}{\rho_l/M^{H_2O} - C^W_{\text{sat}}} \tag{8}$$

where C^W_{sat} is the saturation molar concentration of water vapor at the cell temperature.

The kinematic viscosity of the mixture is defined as

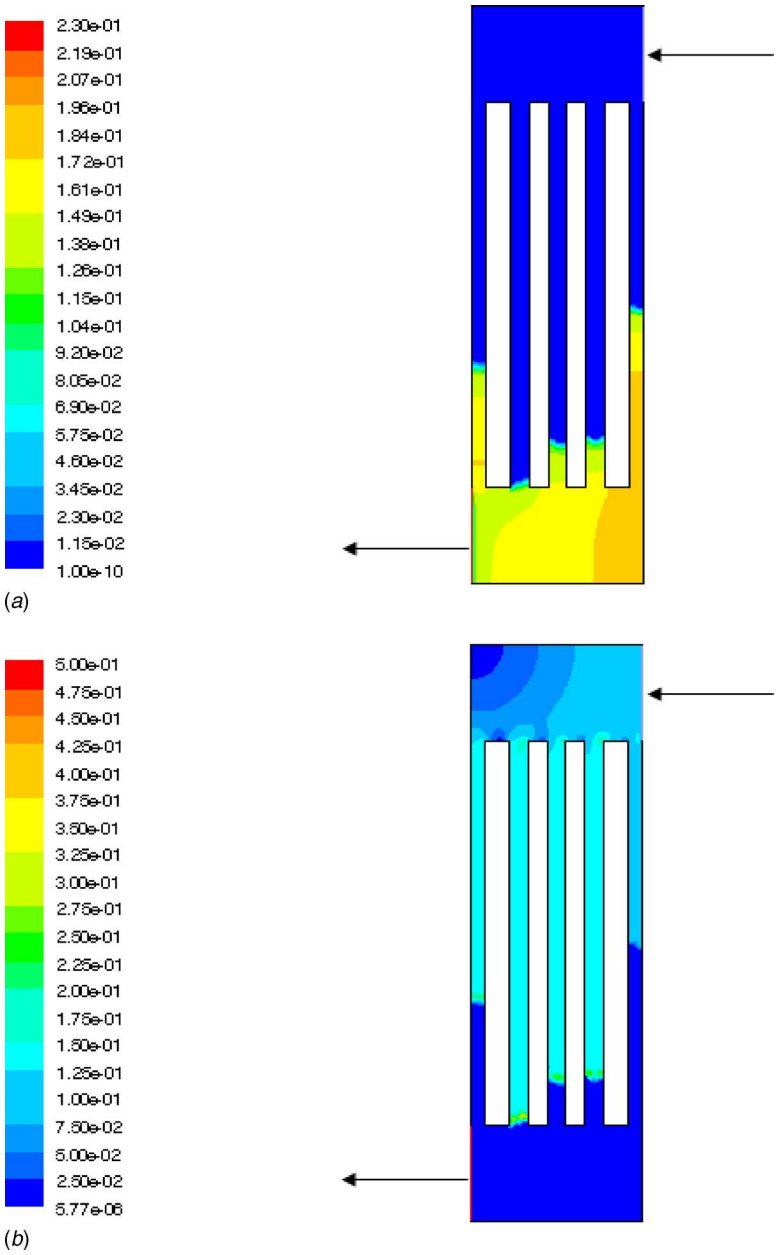

Fig. 11 (***a***) **Saturation contour (20% intrusion, *I*=0.2 A/cm^2, St=4.0);** (***b***) **Velocity (m/s) contour (20% intrusion, *I*=0.2 A/cm^2, St=4.0)**

$$\nu = \left(\frac{k_{\mathrm{rl}}}{\nu_l} + \frac{k_{\mathrm{rg}}}{\nu_g} \right)^{-1} \tag{9}$$

where ν_l and ν_g are the kinematic viscosities of water in liquid and vapor phase, respectively, while k_{rl} and k_{rg} are the relative permeabilities of liquid and vapor phase, respectively.

In Eq. (3), the convective correction factor is defined as

$$\gamma_c = \frac{\rho}{C^W} \left(\frac{\lambda_l}{M^{\mathrm{H_2O}}} + \frac{\lambda_g}{\rho_g} C^W_{\mathrm{sat}} \right) \tag{10}$$

where the relative movements are defined as

$$\lambda_l = \frac{k_{rl}/v_l}{k_{\mathrm{rl}}/v_l + k_{\mathrm{rg}}/v_g} \quad \text{and } \lambda_g = 1 - \lambda_l \tag{11}$$

In micro and minichannels, a certain amount of water, once accumulated, can never be flushed out due to the wall adhesion at the angles. This is called irreducible liquid saturation (s_{ir}). In porous media, this saturation reduces the pore size permanently. Therefore, the relative permeabilities of different phases depend not on the absolute liquid saturation but on the saturation corrected considering the irreducible part. The irreducible liquid saturation can be calculated from the empirical relations [24], where the input is the Bond number (Bo, the ratio of body-force due to gravity in a channel to the surface tension force). The relative permeability of different phases (k_{rl} and k_{rg}) can be modeled through numerical experiments [25,26]. In an upcoming paper, we will present one such model with the predictive capability of pressure-drop in the gas channels of a PEFC.

The cathode inlet flow is assumed to be dry (or at the most fully saturated). The inlet velocity (u_{in}) is calculated in terms of cathode stoichiometry (ξ_c), average current density (I_{av}), inlet density (ρ_{in}), mole fraction of oxygen ($C^{\mathrm{O_2}}$), and the cross section areas of membrane and inlet (A_{mem} and A_{in}, respectively) as follows:

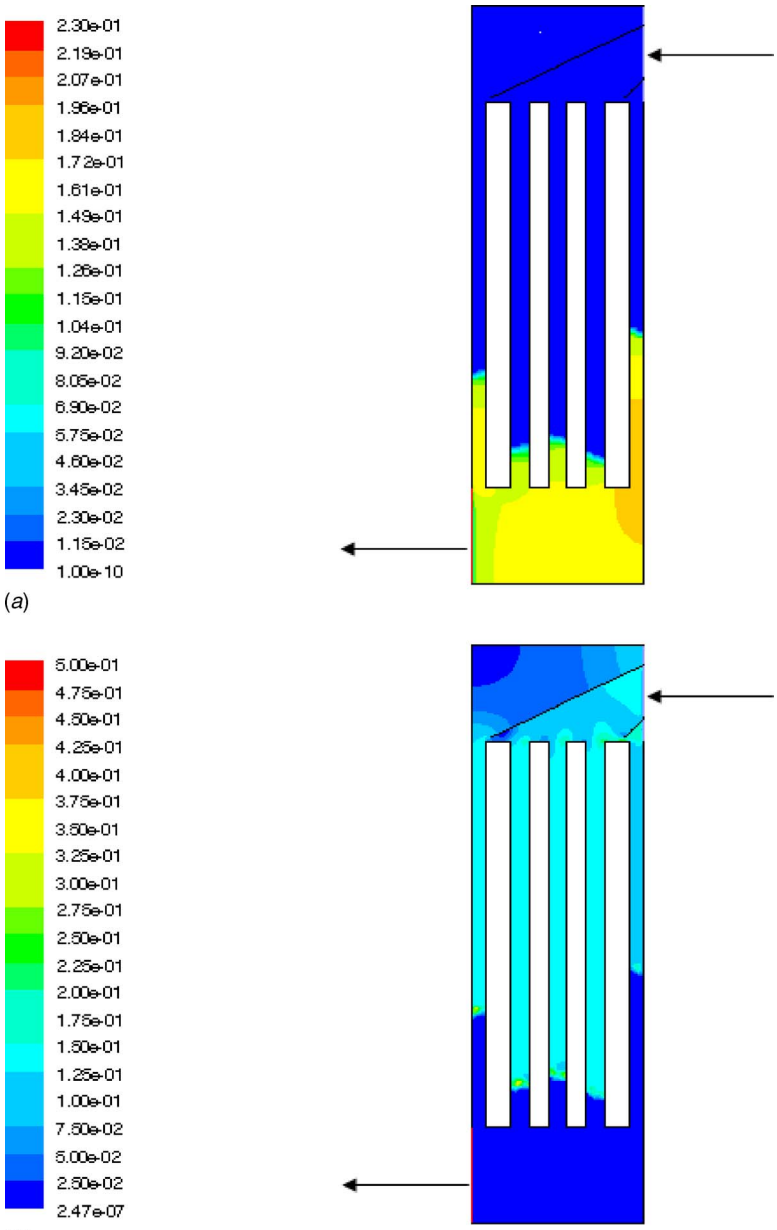

Fig. 12 (*a*) **Saturation contour (20% intrusion with splitters, $I=0.2$ A/cm^2, St=4.0); (*b*) Velocity (m/s) contour (20% intrusion with splitters, $I=0.2$ A/cm^2, St=4.0)**

$$u_{\text{in}} = \frac{\xi_c I_{\text{av}} A_{\text{mem}}}{4FC^{\text{O}_2} A_{\text{in}}} \tag{12}$$

where F is the Faraday constant.

The molar concentrations at the inlet are determined by the inlet pressure and humidity according to the ideal gas law. The exit boundary is assumed to be fully developed such that

$$\frac{\partial \boldsymbol{u}}{\partial n} = 0, \quad p = p_{\text{ref}}, \quad \frac{\partial C^W}{\partial n} = 0 \tag{13}$$

In the present work, the reference pressure is set at 2 atm.

According to the assumption of Darcy's law, the wall boundaries of the gas channel is free of shear. Therefore, at all the walls, we have

$$\boldsymbol{u} \cdot \hat{n} = 0, \quad \frac{\partial p}{\partial n} = 0, \quad \frac{\partial C^W}{\partial n} = 0 \tag{14}$$

Computational Conditions. The computational domain with 20% area maldistribution at the end channels due to GDL intrusion is shown in Fig 3. A straight manifold feeding five parallel channels is considered. Channels are 1 mm wide and 20 mm in length. Pitch of the channels is 2 mm. Depending on the GDL material and channel depth, the GDL intrusion can vary widely from 0% to 40% [27]. In the present case, the cross section area of the end channel is taken to be 20% less than the other channels (which is a representative condition). The manifold is 5 mm in width.

Computations were carried out for a low current density (more prone to channel flooding) and isothermal case with different stoichiometries. The water entry is taken to be equal and constant in all the channels. Even with GDL intrusion this assumption is reasonable. Due to channel flooding and water condensation, the air diffusion in the GDL is hindered and therefore less reaction takes

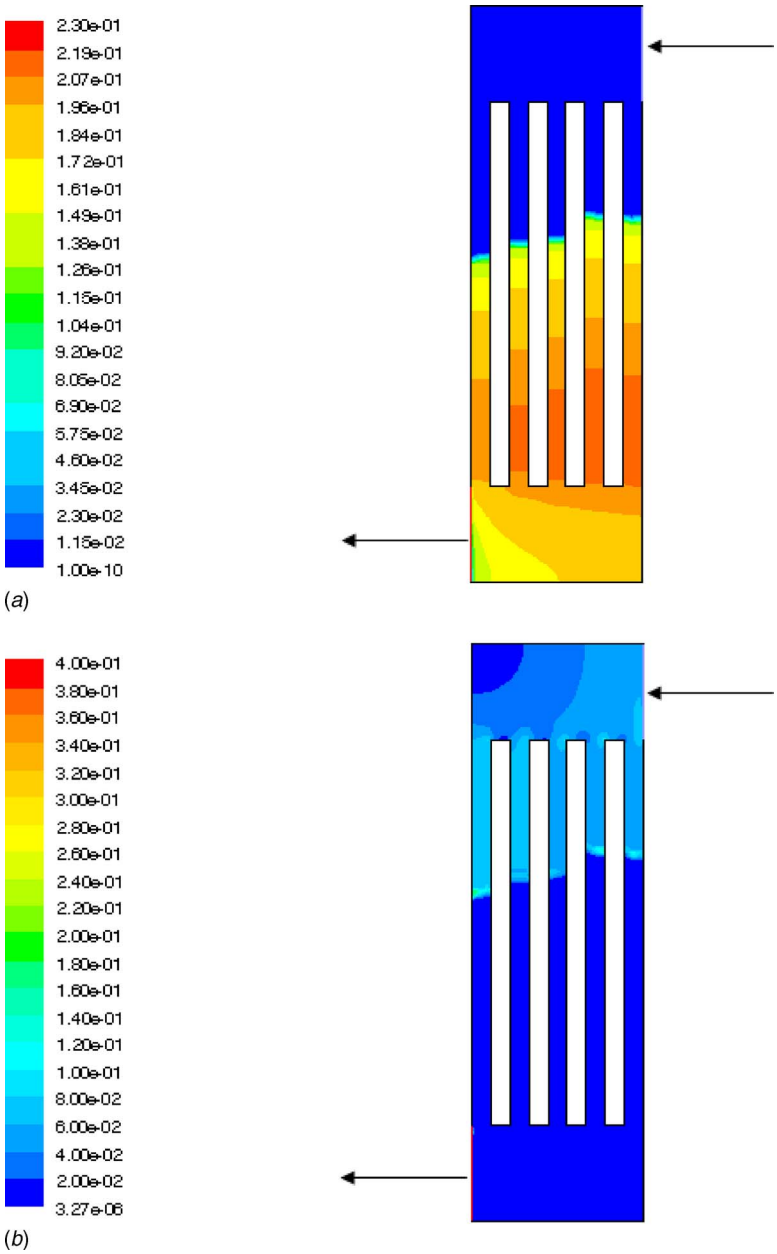

Fig. 13 (*a*) **Saturation contour (no intrusion, I=0.2 A/cm^2, St=2.0); (*b*) Velocity (m/s) contour (no intrusion, I=0.2 A/cm^2, St=2.0)**

place. This eventually decreases the amount of water added to the channels. For this reason, the liquid saturation does not lead to prompt cell death. In the present work, the transient behavior of the liquid-water saturation in the channels is not studied.

A modified design, containing two flow splitters in the inlet header, is also proposed to mitigate the flow maldistribution. These splitters separate the flows in 1:2:1 fraction, a ratio chosen to direct 25% more flow to the intruded channels. The splitters end vertically over the channels at a distance of 0.25 mm, a gap allowing the extra flow directed to the intruded channels to pass through the inner channels. In this way, the flow can dynamically balance itself against varying intrusion. Figure 4 shows the proposed geometry. As a measure of maldistribution, the standard deviation (SD) of the normalized flow through all the channels is used. The flow through any channel is normalized using the average flow through the channels.

Results and Discussion

Single Phase Flow. The system of parallel channels shown in Fig. 3 is meant to supply each channel with the same amount of reactant. Therefore, the standard deviation of the normalized flow through the channels is a good indicator of system performance in uniform distribution of reactants. The lower the standard deviation, the better the system performance. The Reynolds number of the flow, based on inlet width, is 250, a number representing about the middle of the Reynolds number range in practical applications. The commercial computational fluid dynamics (CFD) code, FLUENT version 6.2.16, was used for solving the single-phase flow.

Figure 5 presents the velocity contours in flow channels with 20% area maldistribution, clearly showing the flow maldistribution. In this case, the SD of the normalized flow through the channels is 0.315. The uniformity of the flow is apparent from the

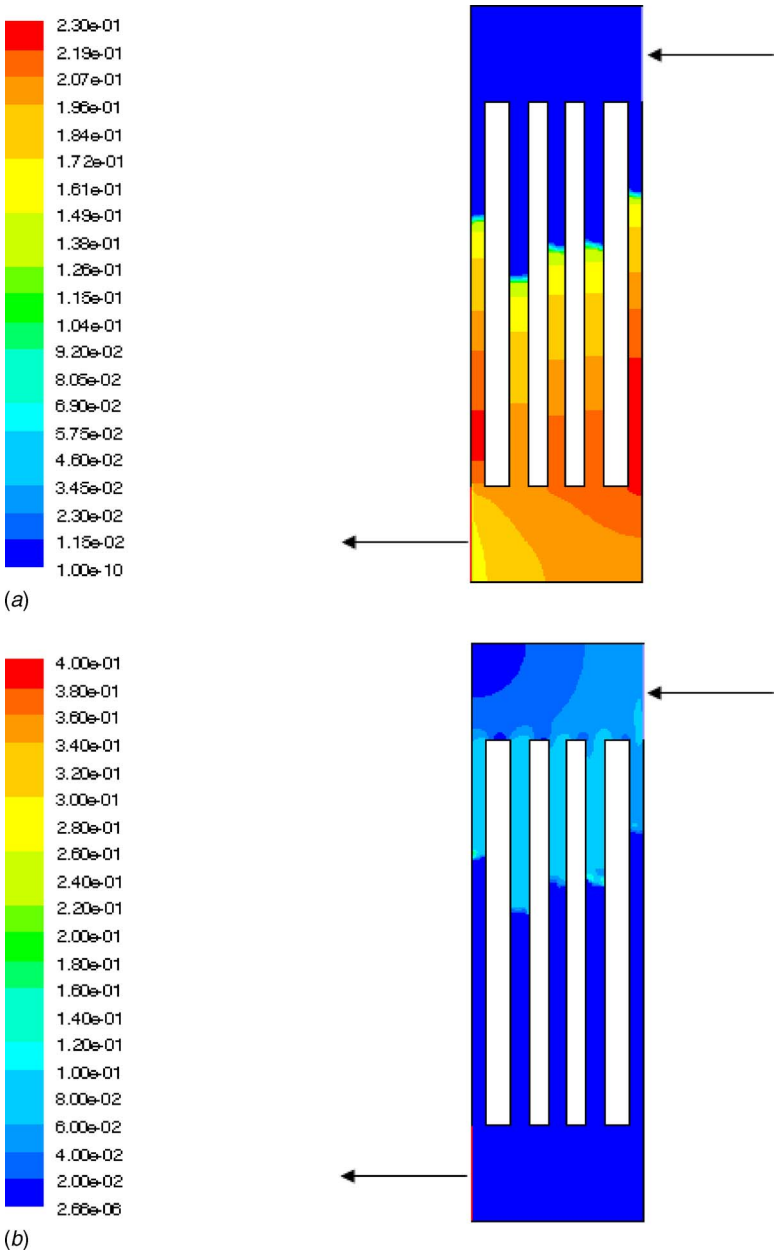

Fig. 14 (*a*) **Saturation contour (20% intrusion, *I*=0.2 A/cm^2, St=2.0);** (*b*) **Velocity (m/s) contour (20% intrusion, *I*=0.2 A/cm^2, St=2.0)**

velocity contours of the proposed model as presented in Fig. 6 and the standard deviation of the normalized flow is 0.133 in this case. Comparison of the standard deviation in the two cases yields a performance improvement of 58%. Performance of this design for the perfectly formed channels was investigated as well. The velocity contours for perfect parallel channels, as displayed in Fig. 7, shows almost uniform flow in the channels with the SD of the normalized flow being 0.129. Use of splitter plates improves the flow distribution by 35% for perfect channels, as shown in Fig. 8. The uniformity of flow distribution with splitters is apparent from the velocity contours. The standard deviation of the normalized flow in this case is 0.084. It is clear that the splitters can ensure a more uniform flow distribution for a wide range of area maldistribution. The SD of the normalized flow is 0.129 in the case of perfect channels, whereas it is 0.133 for the manifold with splitters and 20% area nonuniformity. Hence, we conclude that the splitters can effectively minimize the flow maldistribution due to GDL intrusion. The normalized flow rate through all the channels is plotted for the four cases and the results are presented in Fig. 9. The flow maldistribution is most prominent at the end channels. From the physics of the flow, we can expect this behavior. In the channel adjacent to the inlet, the flow rate would be least due to the strong recirculating vortex at the corner. This would cover most of the channel inlet [8], resulting in a decreased flow rate. The splitter plate directs the flow at an angle so that the corner vortex is suppressed and the streamline-curvature is decreased, and hence higher flow rate is obtained in this channel. In the channel farthest from the inlet, another corner vortex bars the channel inlet. This recirculation occurs because the momentum of the flow that reaches the channel is too low and cannot sustain the adverse pressure gradient. The second splitter directs high momentum flow to the far channel so that it can overcome the corner recirculation and hence, flow maldistribution is alleviated.

Two Phase Flow. Due to the high energy efficiency achievable, low current density is the prime operating range for PEFCs. Chan-

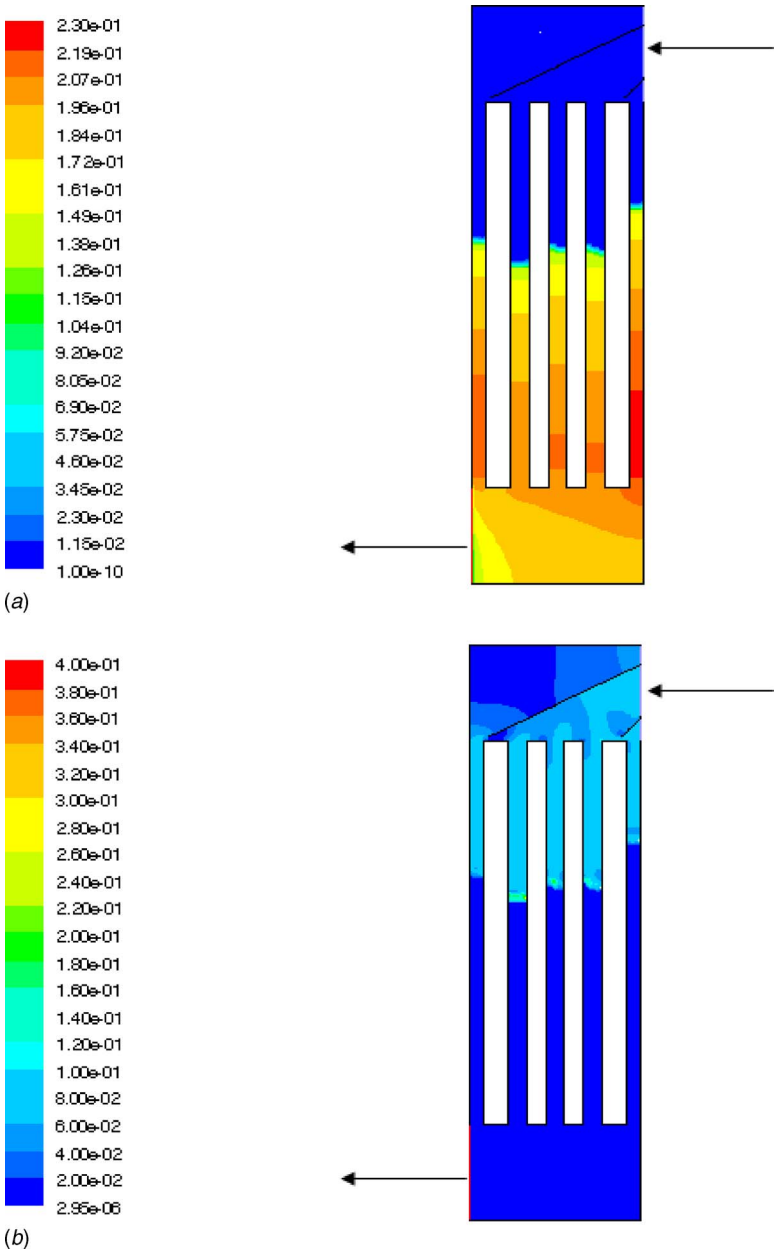

Fig. 15 (*a*) **Saturation contour (20% intrusion with splitters, *I*=0.2 A/cm^2, St=2.0); (*b*) Velocity (m/s) contour (20% intrusion with splitters, *I* =0.2 A/cm^2, St=2.0)**

nel flooding is predominant in these applications due to the low reactant flow rate. From this consideration and as case studies, the two-phase flow in the channels was computed for a current density of 0.2 A/cm^2 and stoichiometries of 4.0 and 2.0. The cell is assumed to operate at a temperature of 80°C whereas the inlet flow has a dew point temperature of 70°C. At this low humidity inlet condition, the gas channel flow has the ability to consume some of the product water in the vapor phase before becoming saturated. Once the flow is saturated by water vapor, excess product water starts to condense. Computations show that the liquid saturation decreases with stoichiometry because the capacity of the gas to carry water is greater at higher flow rate. When computed for the case of 20% GDL intrusion, the end channels seem to become almost entirely flooded. Figure 10(*a*) shows the liquid saturation contours for the case of 0.2 A/cm^2 and a stoichiometry of 4.0 with perfect channels. In this case, the channels are not flooded and the condensation front of liquid water is far downstream. For the channel with highest velocity, it is even possible to flush out all the liquid water. The velocity contours, as displayed in Fig. 10(*b*), show an abrupt deceleration at the condensation front. This is expected from the mass conservation point of view. However, this situation changes drastically as the GDL intrusion is considered. From Fig. 11(*a*), it is clear that for a 20% intrusion of GDL at the end channels, liquid water condenses at the end channels far upstream. As the velocity is the lowest in the channel closest to the inlet (displayed in Fig. 11(*b*)), it experiences condensation before all other channels and eventually gives rise to the maximum liquid saturation.

Figures 12(*a*) and 12(*b*) display the liquid water and velocity contours for the low current density high stoichiometry operating condition (*0.2* A/cm^2 and stoichiometry of 4.0) with flow splitters in place. Using the flow splitters, it is possible to achieve a more uniform velocity distribution in the channels. Even then, the end channels experience higher liquid saturation, although the liquid

Table 1 Maximum liquid saturation at different operating conditions

Stoichiometry	2.0	4.0
Prefect Channels	0.2146	0.1771
Channels with GDL intrusion	0.2289	0.1949
Channels with GDL intrusion and flow splitter	0.2229	0.1885

condensation front is pushed downstream and the maximum liquid saturation is reduced. From Figure 12(*b*), it is clear that velocity distribution is almost uniform in all the channels, but due to higher resistance in the end channels, liquid cannot be flushed out. At low stoichiometry (stoichiometry=2.0), the situation is greatly exacerbated. Even for perfect channels, the condensation starts upstream and it reaches a much higher value. From the liquid saturation contours displayed in Fig. 13(*a*), all the channels other than the channel farthest from the inlet (the channel with highest velocity) are found to be flooded with liquid water. The velocity contours, as shown in Fig. 13(*b*), show a trend similar to the earlier operating conditions, but here, the velocity magnitudes are much smaller. From Fig. 14(*a*), it is clear that when GDL intrusion is considered, the maximum liquid saturation increases even further, although the liquid condensation interfaces do not move appreciably upstream. At the same time, the velocity contours, as displayed in Fig. 14(*b*), show increased maldistribution. These liquid saturation contours indicate that the channels are flooded. At this high liquid saturation, oxygen transport will be seriously hindered, resulting in less reaction and ultimately in cell death.

Using flow splitters can alleviate this extreme condition. From Fig. 15(*a*), it clearly shows that the maximum liquid saturation occurs only in the channel closest to the inlet and the velocity contours displayed in Fig. 15(*b*) show minimum flow maldistribution among the channels. The maximum liquid saturation increases due to GDL intrusion, but the use of splitters can arrest that significantly. The maximum liquid saturations for different cases are tabulated in Table 1. For both the stoichiometries, flow splitters can negate the increase in the saturation level due to GDL intrusion by at least 33%. At lower stoichiometry, the effect of flow splitter is found to be markedly higher.

Conclusions

A two-phase flow model, which is based on the M^2 formalism, was developed and employed to examine the effects of GDL intrusion and manifold design on flow maldistribution among PEFC channels. GDL intrusion in the gas channels and fluid friction were found to cause severe flow maldistribution in parallel flow channels. Results from our computational studies demonstrate that such flow maldistribution can be alleviated by employing flow splitters in the inlet manifold to direct more flow to the most affected channels. It is further shown that flow splitters can reduce flow maldistribution in parallel channels by more than 50% when there is single-phase flow. In the two-phase flow regime, the increment in the maximum liquid saturation due to GDL intrusion in gas channels is lowered by more than one-third.

It should be pointed out that our computational results need to be validated by experiments in order to determine the effects of flow splitters on reducing flow maldistribution in real-world fuel-cell applications. Although only steady-state and isothermal operations were considered in the present study, work is underway to incorporate transient nonisothermal behaviors into the current model and to couple it with a full fuel-cell model.

Acknowledgment

This work was funded in part by Sandia National Laboratories. Sandia is a multiprogram laboratory operated by Sandia Corporation, a Lockheed Martin Company, for the United States Department of Energy's National Nuclear Security Administration under Contract No. DE-AC04-94AL85000.

Nomenclature

A = area
Bo = Bond number
C_i = local concentration of species i, $\mathrm{mol/m^3}$
D_i = diffusion coefficient of species i, $\mathrm{m^2/s}$
d = diameter
F = Faraday's constant, 96,487 C/mol
g = acceleration due to gravity $(\mathrm{m/s^2})$
I = current density, $\mathrm{A/cm^2}$
j = flux
K = permeability of the porous media
k = relative permeability of the phase
M = molecular weight
mf = mass fraction
n = normal direction
P = pressure, Pa
R = universal gas constant, 8.314 J/mol K
RH = relative humidity
S = source term in the governing equations
s = liquid saturation
u = velocity

Greek Letters

α = net water transport coefficient
ρ = density
ε = porosity
Φ = two-phase pressure-drop coefficient
γ = correction factor
λ = relative mobility
s = surface tension coefficient (N/m)
ξ = stoichiometry at gas channel inlet (anode or cathode)
ν = kinematic viscosity

Subscripts and Superscripts

g = gas phase
W = water species
eff = effective
l = liquid
m = mass
sat = saturation
r = relative
c = convective correction
mem = membrane
in = inlet
ir = irreducible
ph = phase
av = average
O_2 = oxygen
H_2 = hydrogen

References

[1] Yin, J. M., Bullard, C. W., and Hrnjak, P. S., 2002, "Single-Phase Pressure Drop Measurements in a Microchannel With Heat Exchangers," Heat Transfer Eng., **23**, pp. 3–12.
[2] Maharudrayya, S., Jayanti, S., and Deshpande, A. P., 2005, "Flow Distribution and Pressure Drop in Parallel-Channel Configurations of Planar Fuel Cells," J. Power Sources, **144**, pp. 94–106.
[3] Hrnjak, P., 2004, "Developing Adiabatic Two Phase Flow in Headers-Distribution Issue in Parallel Flow Micro-Channel Heat Exchangers," Heat Transfer Eng., **25**(3), pp. 61–68.
[4] Webb, R. L., and Chung, K., 2005, "Two Phase Flow Distribution to Tubes of Parallel Flow Air-Cooled Heat Exchangers," Heat Transfer Eng., **26**(4), pp. 3–18.
[5] Chiba, T., and Toshihara, T., 1999, "Heat Exchanger With a Distribution Device Capable of Uniformly Distributing a Medium to a Plurality of Exchanger Tubes," U. S. Patent No. 5,979,547.

[6] Haussman, R., 2001, "Distributing Collecting Tank for the Least Dual Flow Evaporator to a Motor Vehicle Air Conditioning System," U. S. Patent No. 6,199,401 B1.
[7] Lee, E. S., Hidrovo, C. H., Steinbrenner, J. E., Wang, F., Vigneron, S., Goodson, K., and Eaton, J. K., 2005, "Flow Structure and Frictional Characteristics on Two-Phase Flow in a Microchannel in PEM Fuel Cells," *Proceedings of FEDSM 2005, ASME Fluids Engineering Division Summer Meeting and Exhibition*, Houston, TX, Jun. 19–23.
[8] Barrears, F., Lozano, A., Valiano, L., Marin, C., and Pascau, A., 2005, "Flow Distribution in a Bipolar Plate of a Proton Exchange Membrane Fuel Cell: Experiments and Numerical Simulation Studies," J. Power Sources, **144**, pp. 54–66.
[9] Yoon, Y., Lee, W., Park, G., Yang, T., and Kim, C., 2004, "Effects of Channel Configurations of Flow Field Plates on the Performance of a PEMFC," Electrochim. Acta, **50**(2–3), pp. 709–712.
[10] Shimpalee, S., Greenway, S., and Van Zee, J. W., 2006, "The Impact of Channel Path Length on PEMFC Flow-Field Design," J. Power Sources, **160**(1), pp. 398–406.
[11] Li, X., Sabir, I., and Park, J., 2007, "A Flow Channel Design Procedure for Pem Fuel Cells With Effective Water Removal," J. Power Sources, **163**(2), pp. 933–942.
[12] He, G., Ming, P., Zhao, Z., Abudula, A., and Xiao, Y., 2007, "A Two-Fluid Model for Two-Phase Flow in PEMFCs," J. Power Sources, **163**(2), pp. 864–873.
[13] Quan, P., and Lai, M., 2007, "Numerical Study of Water Management in the Air Flow Channel of a PEM Fuel Cell Cathode," J. Power Sources, **164**(1), pp. 222–237.
[14] Jiao, K., Zhou, B., and Quan, P., 2006, "Liquid Water Transport in Parallel Serpentine Channels With Manifolds on Cathode Side of a PEM Fuel Cell Stack," J. Power Sources, **154**(1), pp. 124–137.
[15] Liu, X., Guo, H., Ye, F., and Ma, C. F., 2007, "Water Flooding and Pressure Drop Characteristics in Flow Channels of Proton Exchange Membrane Fuel Cells," Electrochim. Acta, **52**(11), pp. 3607–3614.
[16] Spernjak, D., Prasad, A. K., and Advani, S. G., 2007, "Experimental Investigation of Liquid Water Formation and Transport in a Transparent Single-Serpentine PEM Fuel Cell," J. Power Sources, **170**(2), pp. 334–344.
[17] Zhu, X., Sui, P. C., and Djilali, N., 2007, "Dynamic Behaviour of Liquid Water Emerging From a GDL Pore Into a PEMFC Gas Flow Channel,"J. Power Sources, **172**(1), pp. 287–295.
[18] Wang, X., Duan, Y., and Yan, W., 2007, "Numerical Study of Cell Performance and Local Transport Phenomena in PEM Fuel Cells With Various Flow Channel Area Ratios," J. Power Sources, **172**(1), pp. 265–277.
[19] Wang, C. Y., and Cheng, P., 1996, "A Multiphase Mixture Model for Multiphase, Multicomponent Transport in Capillary Porous Media—I: Model Development," Int. J. Heat Mass Transfer, **39**, pp. 3607–3618.
[20] Cheng, P., and Wang, C. Y., 1996, "A Multiphase Mixture Model for Multiphase, Multicomponent Transport in Capillary Porous Media—II: Numerical Simulation of the Transport of Non-Aqueous Phase Liquids in the Unsaturated Subsurface," Int. J. Heat Mass Transfer, **39**, pp. 3619–3632.
[21] Wang, Y., and Wang, C. Y., 2005, "Modeling Polymer Electrolyte Fuel Cells With Large Density and Velocity Changes," J. Electrochem. Soc., **152**, pp. A445–A453.
[22] Springer, T. E., Zawodzinski, T. A., and Gottesfeld, S., 1991, "Polymer Electrolyte Fuel Cell Model," J. Electrochem. Soc., **138**, pp. 2334–2341.
[23] Wang, Y., Basu, S., and Wang, C. Y., 2008, "Modeling Two-Phase Flow in PEM Fuel Cell Channels," J. Power Sources, **179**(2), pp. 603–617.
[24] Saez, A. E., and Carbonell, R. G., 1985, "Hydrodynamic Parameters for Gas-Liquid Concurrent Flow in Packed Beds," AIChE J., **31**, pp. 52–62.
[25] Dullien, F. A., 1992, *Porous Media: Fluid Transport and Pore Structure*, 2nd ed., Academic, New York, pp. 373–378.
[26] Brooks, R. H., and Corey, A. T., 1964, "Hydraulic Properties of Porous Media," *Hydrology Papers, Colorado State University*, Vol. 3.
[27] Rapaport, P., Lai, Y., and Ji, C., 2006, "GDM Intrusion Into Reactant Gas Channels and the Effect on Fuel Cell Performance," *The Fourth International Conference on Fuel Cell Science and Technology*, Irvine, CA, Jun. 19–21.